VOL. 11, NO. 8, APRIL 2016 ISSN 1819-6608
ARPN Journal of Engineering and Applied Sciences

www.arpnjournals.com

HEAT TRANSFER CHARACTERISTIC OF NANOFLUIDS ON MHD STAGNATION-POINT FLOW TOWARDS STRETCHING OR SHRINKING PLATE IN THE PRESENCE OF INJECTION OR SUCTION

Ashwin Kumar E. N.[1], Norasikin Binti Mat Isa[1], Vibhu Vignesh B.[1] and Kandasamy R.[2]
[1]Faculty of Mechanical and Manufacturing Engineering
[2]Faculty of Science, Technology and Human Development, Universiti Tun Hussein Onn Malaysia, Johor, Malaysia
E-Mail: ashwinkumaren@gmail.com

ABSTRACT

In this paper, the behaviour of three different nanofluids (Cu, Al_2O_3 and TiO2-water) on a stagnation-point flow and heat transfer over a porous vertical shrinking/stretching surfaces for suction/injection are analysed. It is important to note that the order of magnitude of the variation in the temperature profiles depends on the nanoparticles as they have different physical and mechanical properties such as dynamic viscosity, density, specific heat capacity and thermal conductivity. The Navier-Stokes equations for incompressible viscous flow are transformed by similarity transformation into a system of high order ODE that are executed numerically using MAPLE 18 software. The effects of various controlling parameters on (Cu, Al_2O_3 and TiO_2-water) nanofluids are studied. The present results for special cases are found to be in good agreement with previously published works. Copper nanofluid is found to be the most reliable amongst the three nanofluids and best suited for stagnation-point flow towards a porous surfaces.

Keywords: nanofluids, porous medium, thermal radiation, Eckert number, magnetic field and heat source / sink.

INTRODUCTION

Nanofluids are just future possibilities to describe a fluid in which nanometer-sized particles are suspended in conventional heat transfer fluids such aswater, ethylene glycol, oil. These conventional fluids have very poor thermal conductivity, which plays a vital role in heat transfer applications. In past two decades, researchers have been working to increase the heat transfer capacity of conventional fluids by introducing different nanoparticles such as metals(Cu, Al, Au), oxides (CuO, Al_2O_3, TIO_2, ZnO), etc. The concept of nanofluid, which is a new kind of modern heat transfer fluid, has been advanced by Choi (1995), who showed substantial augmentation of heat, transported in suspensions of Cu nanoparticles in heat transfer fluids and observed that the thermal conductivity of conventional fluids have increased. Pak and Cho (1998) studied the heat transfer performance of Al_2O_3 and TiO_2 nanoparticles dispersed in water flowing in a horizontal circular tube. They found that the Nusselt number of nanofluids increased with an increase in the Reynolds number as well as the volume fraction. Heris *et al.* (2006, 2007) illustrated the convective heat transfer behaviour of (Al_2O_3 and CuO–water) nanofluids for laminar flow in an annular tube subjected to a constant wall temperature boundary condition. The results proved that the heat transfer characteristics increased with an increasing Peclet number as well as volume fraction and the Al_2O_3–water nanofluid showed larger enhancement than CuO–water nanofluid. Duangthongsuk andWongwises (2009) have discussed the Heat transfer enhancement and pressure drop characteristics of TiO_2–water Nanofluid in a heat exchanger. This article elucidates the heat transfer characteristics and flow characteristics of (Cu, TiO_2, Al_2O_3–water) nanofluids on a stagnation-point flow and heat transfer over vertical porous shrinking/stretching surfaces under laminar flow conditions

MHD nanofluid flow is the study of electrically conducting nanofluids movement. The behaviour of MHD flow of an electrically conducting fluid towards a stretching/shrinking plate is important in modern metallurgy and metal-working processes. Stagnation flow of a Newtonian fluid over a stretching or shrinking platehas great significant in many industries, such as the aerodynamic extrusion of plastic sheets, continuous stretching of plastic films and artificial fibers, etc. Mahapatraand Gupta (2002) has presented a paper on the heat transfer in stagnation-point flow towards a stretching palte. Wang (2008) studied the steady stagnation-point flow over a shrinking plate. The Navier–Stokes equations which are generally in PDE are reduced to ODE using similarity transformation and then solved numerically. Mostafa *et al.* (2011) investigated stagnation point flow of a nanofluid towards a stretching sheet. Ibrahim *et al.*(2013) have presented paper on stagnation point flow and heat transfer due to nanofluid towards a stretching sheet under the influence of magnetic field. Finally, we mention an interesting papers by Fang *et al.* (2009), where the Newtonian flow over an unsteady shrinking plate with mass transfer has been numerically studied.

The objective of the present work is to investigate the stagnation-point flow and heat transfer characteristic in permeable stretching/shrinking surface. In this paper, the effects of Grashof number, Eckert number, thermal radiation, magnetic field strength and heat generation/absorption under the influence of injection or suction on temperature fields for three nanofluids using the thermo-physical properties of nanoparticles and of the base fluid (water) has been studied.

MATHEMATICAL ANALYSIS

The flow model for achieving our objectives is shown in Figure-1. In this study, the nanofluid flow selected is a 2-D stagnation-point flow, over a permeable plate. The plate is subjected to shrinking and stretching and the flow is analysed in each plates. For stretching plate the linear velocity over a porous plate is $u_w = cx$ and the velocity over a porous plate becomes negative for shrinking plate that is$u_w = -cx$. The flow is time independent and laminar flow. $U(x) = ax$ is defined as the free stream flow. Magnetic field strength (B_0) which is present in positive x-axis, influences the nanofluid flow. Nanoparticles and base fluids areassumed tobeinthermal equilibrium and no slip occurs between them. The acceleration due to gravity is denoted by g. The thermo-physical properties of base fluid and nanoparticles is given in Table-1. Prandtl number of water is taken as 6.2 at 20℃.

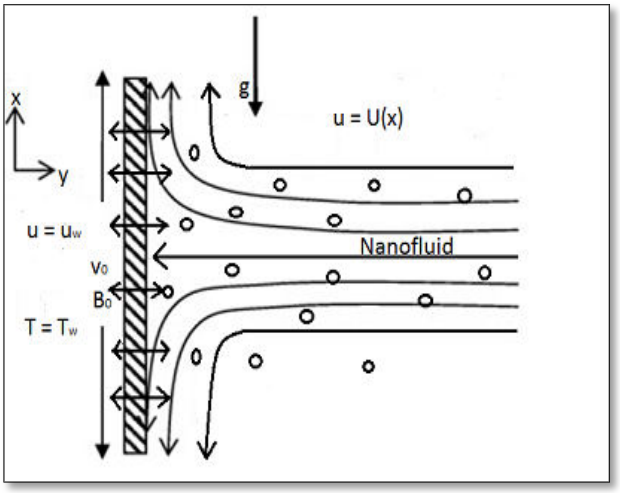

Figure-1. Stagnation-point flow model over a vertical permeable plate.

Table-1. Thermo-physical properties of fluid and nanoparticles(Oztopand Abu-Nada, 2008).

Physical properties	Water	Cu	Al_2O_3	TiO_2
Cp(J/KgK)	**4179**	**385**	**765**	**686.2**
ρ(Kg/m^3)	997.1	8933	3970	4250
κ (W/mK)	0.613	401	40	8.9538

With above assumptions, the boundary layer equations are as follows:

$$\frac{\partial u}{\partial x} + \frac{\partial v}{\partial y} = 0 \quad (1)$$

$$u\frac{\partial u}{\partial x} + v\frac{\partial v}{\partial y} = U(x)\frac{dU(x)}{dx} + \frac{\mu_{nf}}{\rho_{nf}}\frac{\partial^2 u}{\partial y^2} + \frac{\mu_{nf}}{\rho_{nf}K}(U(x) - u) \quad (2)$$

$$u\frac{\partial T}{\partial x} + v\frac{\partial T}{\partial y} = \alpha_{nf}\frac{d^2T}{dy^2} + \frac{Q_0}{(\rho C_p)_{nf}}(T - T_\infty) - \frac{1}{(\rho C_p)_{nf}}\frac{\partial q_r}{\partial y} + \frac{\mu_{nf}}{(\rho C_p)_{nf}}\left(\frac{\partial u}{\partial y}\right)^2 \quad (3)$$

Subjected to the boundary conditions (for shrinking or stretching plate)

$$v = v_0, u = u_w(x) = \pm cx, T = T_w \text{ at } y = 0; \quad T \to T_\infty, u \to U(x) = ax, C \to C_\infty \text{ as } y \to \infty \quad (4)$$

For calculating density, thermal conductivity, dynamic viscosity, thermal diffusivity and heat capacitance of nanofluids the below mentioned equations are used.

$$\rho_{nf} = (1 - \phi)\rho_f + \phi\rho_s \quad (5)$$

$$\kappa_{nf} = \kappa_f\left[\frac{\kappa_s + 2\kappa_f - 2\phi(\kappa_s - \kappa_f)}{\kappa_s + 2\kappa_f + 2\phi(\kappa_s - \kappa_f)}\right] \quad (6)$$

$$\mu_{nf} = \frac{\mu_f}{(1-\phi)^{2.5}} \quad (7)$$

$$(\rho C_p)_{nf} = (1 - \phi)(\rho C_p)_f + \phi(\rho C_p)_s \quad (8)$$

$$\alpha_{nf} = \frac{\kappa_{nf}}{(\rho C_p)_{nf}} \quad (9)$$

Equation. (1) to Equation. (3) is transformed using similarity functions, the stream function are

$$\psi = \sqrt{c \cdot \nu_f} \cdot f(\eta) \cdot x, \eta = \sqrt{\frac{c}{\nu_f}} \cdot y, \quad (T_W - T_\infty)\,\theta(\eta) = T - T_\infty \quad (10)$$

$$\theta_w = \frac{T_w}{T_\infty} \quad (11)$$

Defining the stream function ψ that is, (u) = ψ_y,

(v) = -ψ_x , which satisfies the Equation. (1)and Equation. (5) to Equation. (9) are substituted into Equation. (2), Equation. (3) and Equation. (4),we get following non-linear ODE:

$$f''' + ((1-\phi)^{2.5}M + K)\left(\frac{a}{c} - f'\right) + (1-\phi)^{2.5}\left(1-\phi+\phi\frac{\rho_s}{\rho_f}\right)\left(\frac{a^2}{c^2} + ff'' - f'^2 + \gamma\theta\right) = 0 \quad (12)$$

$$\theta'' + \frac{Pr}{\left(\frac{\kappa_{nf}}{\kappa_f} + N(1+(\theta_w-1)\theta)^3\right)} \cdot \left[\frac{3N}{Pr}.(\theta_w-1)(1+(\theta_w-1)\theta)^2\theta'^2 + \left(1-\phi+\phi\frac{(\rho c_p)_s}{(\rho c_p)_f}\right)(F\theta' - 2F'\theta) + \lambda\theta + \frac{Ec}{(1-\phi)^{2.5}}\theta'\right] = 0 \quad (13)$$

Boundary conditions for stretching and shrinking plate:

$$\left.\begin{aligned} &f = S, f' = 1, \theta = 1 \text{ at } \eta = 0 \text{ (stretching)} \\ &f = S, f' = -1, \theta = 1 \text{ at } \eta = 0 \text{ (shrinking)} \end{aligned}\right\} \text{asy=0}$$
$$f' \to \frac{a}{c}, \theta \to 0, \quad \eta \to \infty \quad (14)$$

$Pr = \frac{v}{\alpha}$ is the Prandtl number, $Ec = \frac{{u_w}^2}{C_p \Delta T}$ is the Eckerts number, $Gr = \frac{g\beta(T_W - T_\infty)x^3}{v^2}$ is the Grashof number, $\gamma = \frac{Gr}{Re^2}$ is the Buoyancy parameter, $S = -\frac{v_w}{\sqrt{cv_f}}$ is the injection parameter, $\lambda = \frac{Q_0 v_f}{c\kappa_{nf}}$ is the heat source/sink, $K = \frac{v_f}{cK_1}$ is the porous parameter, $N = \frac{16\sigma^* {T_f}^3}{3k_f K^*}$ is the thermal radiation parameter and $M = \frac{\sigma B_0^2}{\rho_f c}$ is the magnetic parameter.

For validating the results obtained from MAPLE 18 software, the values for the parameters as given in previously presented journals by Mahapatra and Gupta (2002), Hamad and Pop (2010) and Pal *et al*. (2014) are given in MAPLE 18 software to compare heat transfer rate values and velocity profiles. From Table-2, the dimensionless heat transfer rates obtained from MAPLE 18 software is in agreement with previously published journals by Mahapatra and Gupta (2002) and Hamad and Pop (2010). From Figure-2 and Figure-3, the velocity profiles obtained in MAPLE 18 software is in perfect correlation with that of Pal *et al*. (2014) results.

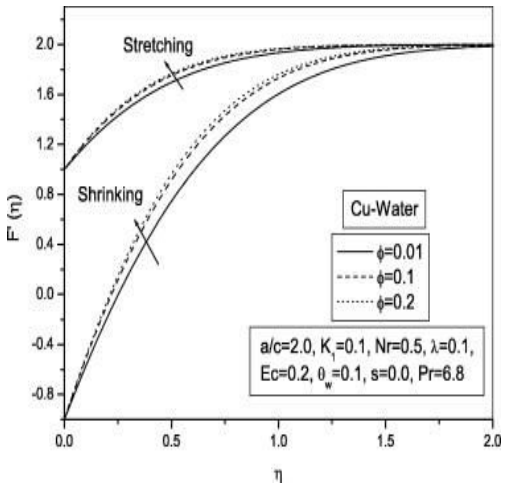

Figure-2. Nanoparticle volume fraction effect on copper nanofluid Pal *et al*. (2014).

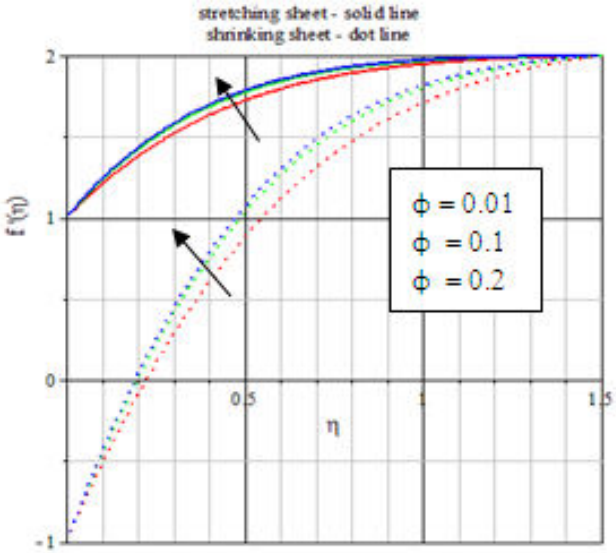

Figure-3. Nanoparticle volume fraction effect on copper nanofluid (MAPLE 18 software).

Table-2. Comparison of –θ'(0) obtained from MAPLE software with published works for stretching plate

Pr	a/c	Mahapatra and Gupta (2002)	Hamad and Pop (2010)	Present results
1	0.1	0.625	0.6216	0.62537
	1	0.796	0.8001	0.79967
	2	1.124	1.1221	1.12375
1.5	0.1	0.797	0.7952	0.79500
	1	0.974	0.7952	0.79503
	2	1.341	1.3419	1.34095

RESULT AND DISCUSSIONS

Equations 12 and 13 are high order nonlinear ordinary differential equations which are solved by using MAPLE 18 software. This software uses a fourth-fifth order Runge–Kutta–Fehlberg method as default to solve boundary value problems numerically using the dsolve command. The thermal conductivity is calculated using the Maxwell equation (6) and tabulated in Table-3. The thermal conductivities of nanofluids increase for increasing nanoparticle volume fraction (ϕ). We have calculated thermal conductivities by changing ϕ up to 0.4 vol%. While simulation, 0.2 vol% is taken for ϕ and studied. The reason is that, during simulation a collective of controlling parameters governs the nanofluid flow. Beyond 0.2 vol%, the governing equation will not converge.

Table-3. Thermal conductivity (κ) of nanofluids for different nanoparticle volume fraction.

Nanoparticle volume fraction (φ) (vol%)	**Thermal conductivity** (κ) (W/mK)			
	Fresh water	**Cu-fresh water**	**Al_2O_3-fresh water**	**TiO_2-fresh water**
0	0.613	0.613	0.613	0.613
0.1	0.613	0.9177	0.9026	0.8532
0.2	0.613	1.4241	1.3713	1.2107
0.3	0.613	2.4311	2.2598	1.7985
0.4	0.613	5.4066	4.5888	2.9455

In Figure-4 shows the corresponding thermal conductivities of nanofluids when (Cu, Al_2O_3 and TiO_2) nanoparticles added to base fluid with the thermal conductivity of base fluid (fresh water). The thermal conductivity consecutively increases as the volume of nanoparticles increases. From the graphs, it is clearly observed that for higher ϕ, Copper nanofluid has more thermal conductivity in both base fluids, followed by Alumina nanofluid and Titanium dioxide nanofluid having lowest thermal conductivity amongst three.

Table-4 shows the stream conditions for Figure-5 to Figure-16 for studying the behaviour of the three nanofluids. Based on the governing parameters mentioned in Table 4, the behaviour of nanofluids is analysed in the presence of both suction and injection. For all governing parameters, a fixed value is taken. Only the parameters to be studied is altered and the chosen value of these parametersare higher than the fixed value of the parameters respectively, for understanding the exact behaviour of that parameter alone.

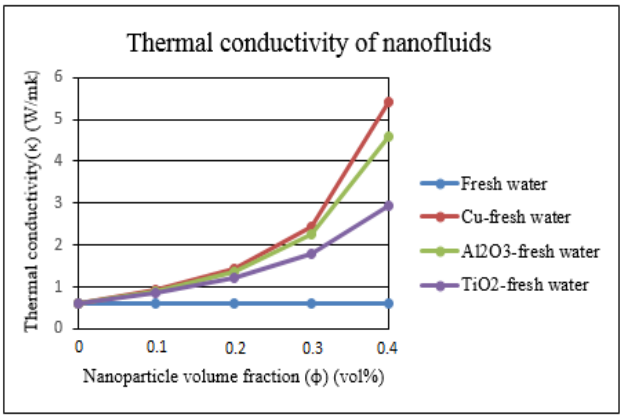

Figure-4. Thermal conductivity (κ) of (Cu, Al_2O_3 and TiO_2–fresh water) nanofluids for different nanoparticle volume fraction.

Table-4. Stream conditions for Figure-5 to Figure-16.

Figures	**Parameters**	**Fixed parameters**
5 - 8	**Magnetic strength (M) = 5**	Pr = 6.2, a/c = 2, ϕ= 0.2, G = 3, K = 0.1, S = -1/1, θ_w = 0.5, M = 1, λ = 0.1, N = 1, Ec = 0.2
9 - 10	Heat source (λ) = 2	
11 - 12	Eckert number (Ec) = 0.4	
13 – 14	Thermal radiation (N) = 5	
15 - 16	Heat sink (λ) = -1	

Figure-5 and Figure-6 presents the effects of magnetic field strength (M) on velocities of three nanofluids. The effect of M is studied mainly on velocities. When comparing Figure-5 and Figure-6, the velocity of Cu-fresh water nanofluid at η = 0.5, is above $f'(\eta)$ = 1.5 in the case of suction but it is below $f'(\eta)$ = 1.5 in case of injection. The effect of M is effective in the case of injection as it has reduced notable difference in the velocity profiles.

The effect of M on TiO_2-fresh water nanofluid and Al_2O_3-fresh water nanofluid show less velocity profiles than the Cu-fresh water nanofluid in both suction and injection. Figure-5, the stretching and shrinking surface initially forming a separate profile and the two profiles merge at $\eta = 1.7$ (Cu-fresh water) and at $\eta = 1.3$ (TiO_2-fresh water and Al_2O_3-fresh water) nanofluids. In Figure-6 the profiles for shrinking and stretching merge at $\eta = 1.1$ (Cu-fresh water) and at $\eta = 1.3$ (TiO_2-fresh water and Al_2O_3-fresh water) nanofluids.

In Figure-7 and Figure-8 temperature profiles are compared between injection and suction respectively in the presence of M. In both injection and suction, shrinking surface shows good temperature profiles compared to the stretching surface. In Figure-7 and Figure-8, there is no significant difference near the thermal boundary layer in the presence of stretching surface. But as the nanofluid moves away from the boundary layer, it is evident that TiO_2-fresh water nanofluid has less temperature comparatively and beyond $\eta = 0.6$ (injection) and $\eta = 0.7$ (suction) temperature increases for Al_2O_3-fresh water nanofluid.

Figure-7 and Figure-8, temperature profiles for shrinking surfaces, forms a peak when the flow is very close to boundary layer, in both suction and injection. TiO_2-fresh water nanofluid has high temperature profile in the presence of injection. In the presence of suction and flow over shrinking surface Cu-fresh water nanofluid has high temperature. During injection, temperature profiles are good as the effect of magnetic field is available, even the flow is away from thermal boundary layer. For suction, the effect of magnetic field on nanofluids is only present when the flow is very close to the boundary layer.

Srivatsava, P., Mallikarjun, B. and Yang, X. (2013). Optimal test sequence generation using firefly algorithm. Swarm and Evolutionary Computation, 8, pp. 44-53.

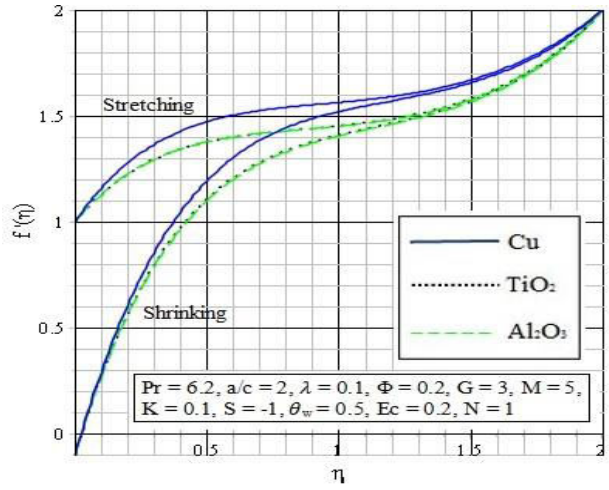

Figure 5: Magnetic field effects on velocity profiles of (Cu, Al_2O_3 and TiO_2–fresh water) nanofluids (Injection)

Heat source ($\lambda>0$) effects on temperature profiles in the presence of injection and suction is given in Figure-9 and Figure-10. Temperature profiles for injection is good when compared to suction. Temperature profiles for both shrinking and stretching tends to zero at $\eta = 2$ in the presence of injection. In suction, temperature profiles becomes zero at $\eta = 1.7$. Its evident from the Figures 9 and 10, the effect of heat source in the presence of injection is achieved in a distance from the thermal boundary layer. In suction, heat source effect on nanofluids is achieved only when the flow is closer to the boundary layer. After $\eta = 0.6$, the temperature gradient is greater for both shrinking and stretching surfaces in the presence of suction compared to shrinking and stretching surfaces in case of injection.

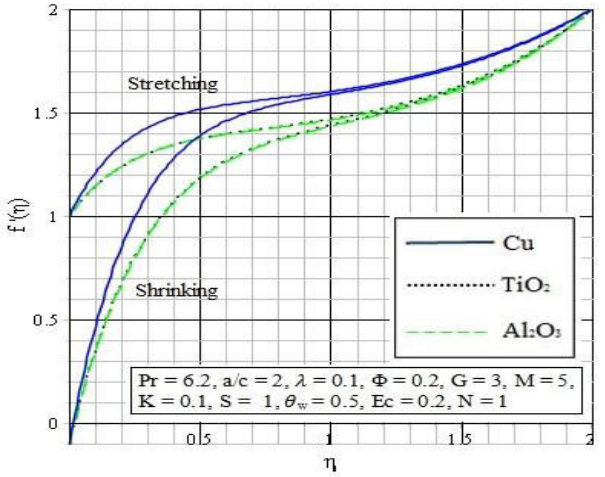

Figure-6. Magnetic field effects on velocity profiles of (Cu, Al_2O_3 and TiO_2–fresh water) nanofluids (Suction).

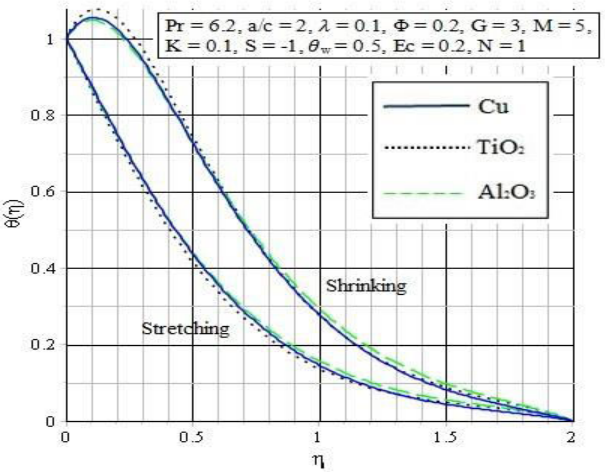

Figure-7. Magnetic field effects on temperature profiles of (Cu, Al_2O_3 and TiO_2–fresh water) nanofluids (Injection).

In Figure-9 and Figure-10, the effect of heat source on temperature profiles is observed. In the presence of injection (S= -1), TiO_2-fresh water nanofluid has high temperature profile for shrinking surface followed by Al_2O_3-fresh water and finally Cu-fresh water. The physical explanation for such behaviour is that the heat source, in which heat capacitance place the major role. TiO_2-fresh

water nanofluid has less heat capacitance when compared to Al_2O_3-water and Cu-fresh water. However in Figure 10, quite opposite results are produced in the presence of heat sink parameter, as Cu-fresh water and TiO_2-fresh water nanofluids have high temperature profiles with no significant differences when the flow is nearer to the boundary layer. When the nanofluid flow is at a distance of $\eta = 0.3$, Al_2O_3-fresh water shows a rise in temperature in shrinking surface. In Figure-9, effects of heat source on all three nanofluids, flowing over stretching sheet has a single profile. In Figure-10, in the presence of suction, TiO_2-fresh water nanofluid has low temperature profile. Figure-11 and Figure-12, depicts the influence of Eckert number (Ec). Ec is nothing but the parameter for viscous dissipation. Viscous dissipation is the frictional loss of energy, when the fluid is sheared. In Figure-11 and Figure-12, in the presence of shrinking surface there is a peak formation in temperature profiles when nanofluid flow is closer to the boundary layer. Temperature profiles for shrinking surfaces is greater than the temperature profiles for stretching surfaces, in both suction and injection. Temperature profiles tends to zero at $\eta = 2$ in the case of injection and $\eta = 1.7$ in the case of suction. As in Figure-11, Cu-fresh water and Al_2O_3-fresh water has temperature profile around $\theta(\eta)=1.4$; TiO_2-fresh water the temperature profile around $\theta(\eta)=1.5$.

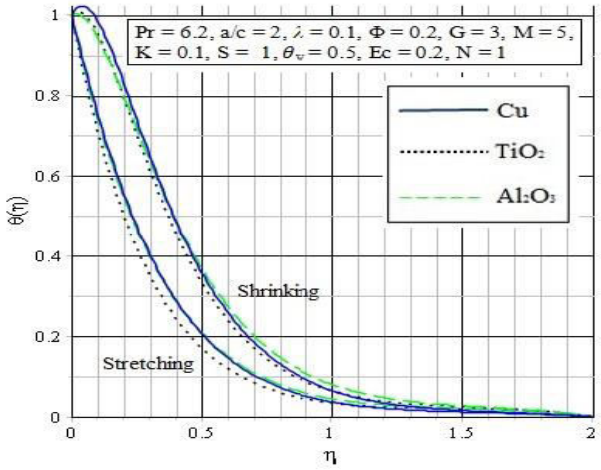

Figure-8. Magnetic field effects on temperature profiles of (Cu, Al_2O_3 and TiO_2–fresh water) nanofluids (Suction).

From Figure-12, for shrinking surface very high profiles for Cu-fresh water and TiO_2-fresh water nanofluids has high temperature; at a distance $\eta = 0.4$ from boundary layer, there is a rise in temperature for Al_2O_3-fresh water, as it shows temperature profiles higher than other two nanofluids. In stretching surface, TiO_2-fresh water has low temperature profile comparatively; Cu-fresh water and Al_2O_3-fresh water nanofluids has no significant changes in temperature profiles in stretching surface, which is clear from Figure-11 and Figure-12.

The effect of thermal radiation (N) is studied on temperature profiles in Figure-13 and Figure-14. Temperature profiles is slightly above $\theta(\eta)=1$, for both suction and injection cases. The temperature gradient in the case of suction is greater compared to temperature gradient in the case of injection. From the influence of N, temperature profiles at $\eta = 1.1$ are above $\theta(\eta)= 0.1$, for both shrinking and stretching surfaces in the presence of injection; temperature profiles in case of suction are below $\theta(\eta)= 0.1$ at the same distance from the boundary layer.

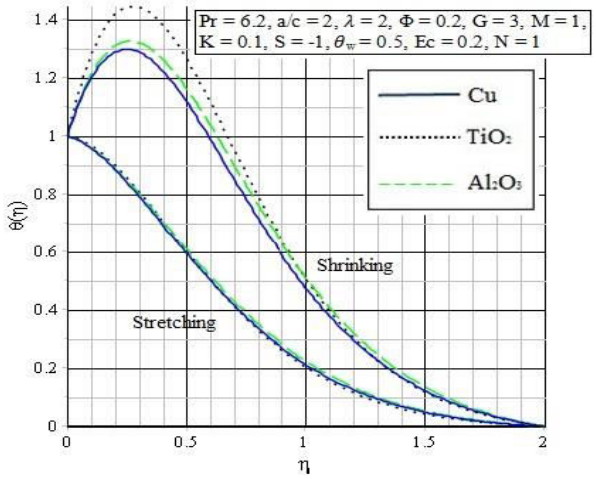

Figure-9. Heat source effects on temperature profiles of (Cu, Al_2O_3 and TiO_2–fresh water) nanofluids (Injection).

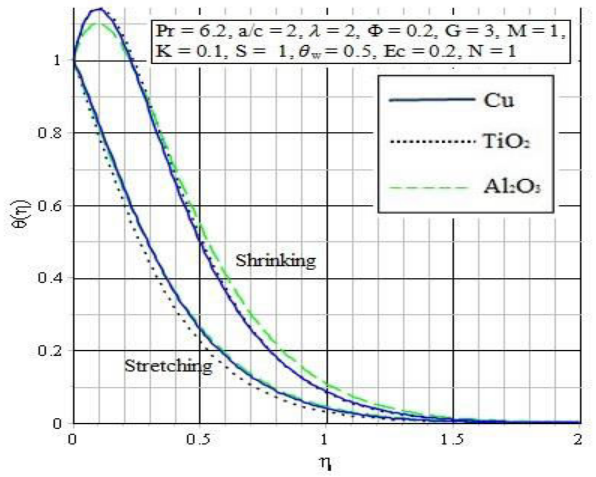

Figure-10. Heat source effects on temperature profiles of (Cu, Al_2O_3 and TiO_2–fresh water) nanofluids (Suction).

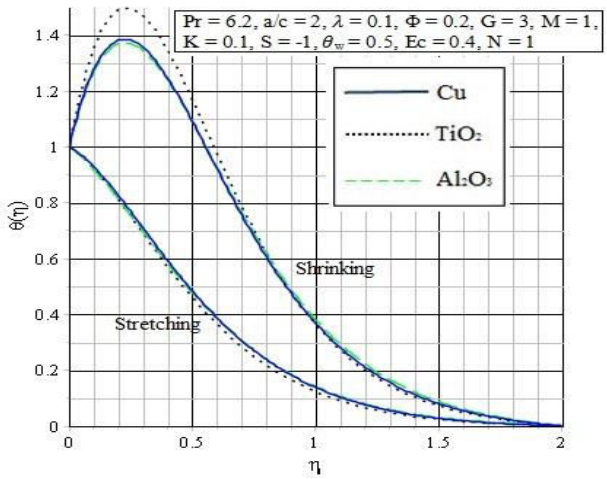

Figure-11. Eckert number effects on temperature profiles of (Cu, Al_2O_3 and TiO_2–fresh water) nanofluids (Injection).

TiO_2-fresh water nanofluid has high temperature profile over shrinking surface in the presence of injection. The explanation of such behaviour is that there is decrease in the divergence of radiative heat flux $\frac{\partial q_r}{\partial y}$ as thermal conductivity (κ) increases. In Figure-4.14, initially Al_2O_3-fresh water nanofluid has low temperature profile, beyond η= 0.5 there is notable rise in temperature profile for Al_2O_3-fresh water nanofluid in shrinking surface. The difference in temperature profiles of the three nanofluids are very close in shrinking and stretching surfaces. In Figure-13, near the thermal boundary layer, TiO_2-fresh water nanofluid over shrinking surface has high temperature profiles; in Figure-14, Cu-fresh water nanofluid over shrinking surfaces shows high temperature profile.

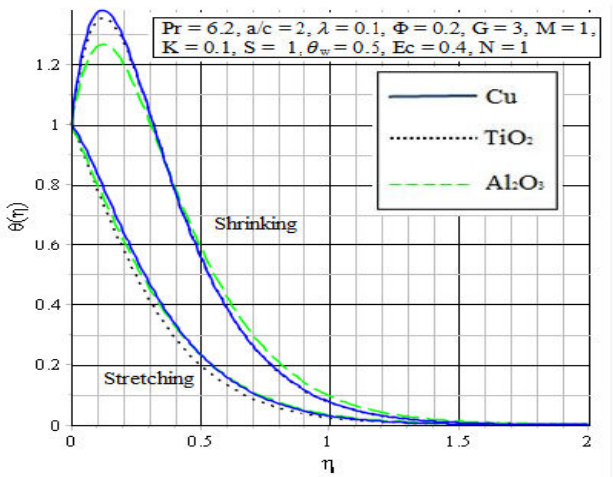

Figure-12. Eckert number effects on temperature profiles of (Cu, Al_2O_3 and TiO_2–fresh water) nanofluids (Suction).

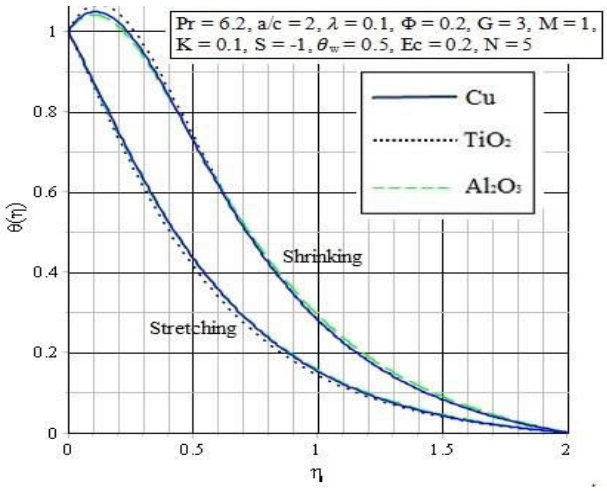

Figure-13. Thermal radiation effects on temperature profiles of (Cu, Al_2O_3 and TiO_2–fresh water) nanofluids (Injection).

Heat sink (λ<0) effect is observed in Figure-15 and Figure-16 in the presence of injection/suction on stagnation-point flow. In the presence of heat sink, temperature profiles are low in both suction as well as injection, when compared to the temperature profiles of heat source that is Figure-9 and Figure-10. The presence of heat sink in the boundary layer absorbs energy which causes the temperature field to decrease. The effect of heat sink in the presence of suction, temperature profiles tends to zero at η= 1.5; in case of injection, profiles tends to zero at η = 2. Shrinking surfaces in Figure-15 and Figure-16 shows small peak in temperature profiles near the thermal boundary layer. The stretching surface does not form peak temperature, it reduces continuously as the flow is away from boundary layer.

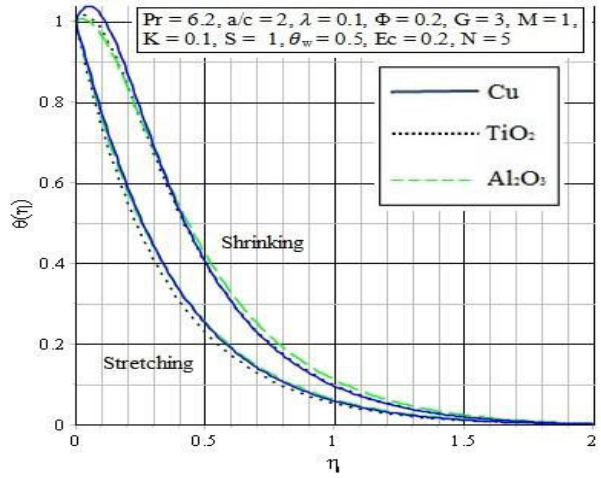

Figure-14. Thermal radiation effects on temperature profiles of (Cu, Al_2O_3 and TiO_2–fresh water) nanofluids (Suction).

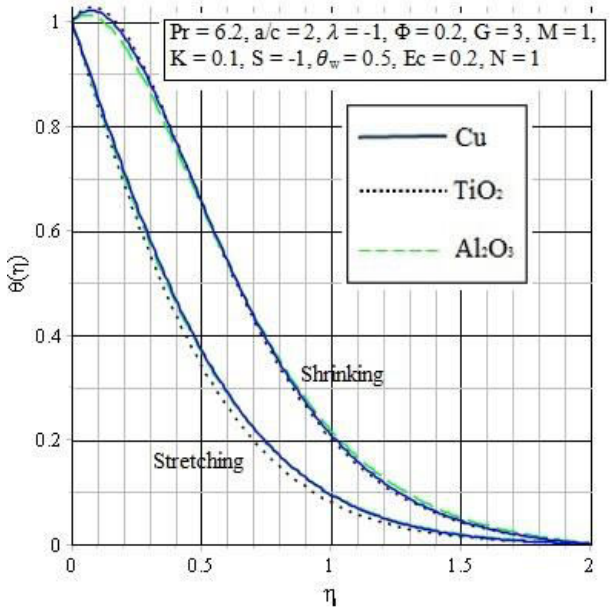

Figure-15. Heat sink effects on temperature profiles of (Cu, Al_2O_3 and TiO_2–fresh water) nanofluids (Injection).

In Figure-15, temperature profiles for shrinking and stretching surface at η = 1 is θ(η)= 0.22 and θ(η)= 0.098 respectively in case of injection. In Figure 16, temperature profiles of shrinking and stretching surfaces are below θ(η)= 0.05 in the presence of suction. In case of suction, when nanofluid flow is over shrinking surfaces Cu-fresh water nanofluid shows high temperature profile near the boundary layer and Al_2O_3-fresh water nanofluid beyond η = 0.5 has a temperature rise. In Figure 15 and Figure 16, TiO_2-fresh water nanofluid has low temperature profiles over stretching surface and temperature profiles of Cu-fresh water and AL_2O_3-fresh water has same temperature distribution over stretching surface.

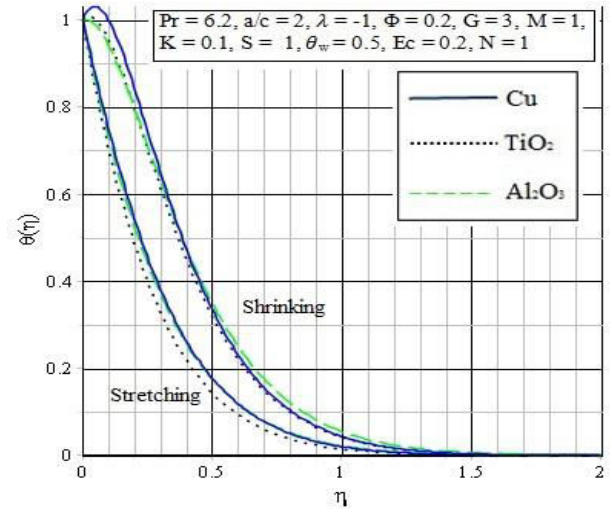

Figure-16. Heat sink effects on temperature profiles of (Cu, Al_2O_3 and TiO_2–fresh water) nanofluids (Suction).

CONCLUSIONS

In the present study, we have discussed theoretically the problem of convective boundary-layer flow of a Newtonian fluid past a permeable stretching or shrinking plate in the presence of suction or injection. Nanoparticle volume fraction plays a vital role in studying the behaviour of nanofluids on temperature distributions. Nanofluids is of great interest in research field because they can be used in variety of applications involving heat transfer and others such as in bio-medical, solar heating, etc.

Different nanofluids have been studied in this paper with the effects of various controlling parameters. Interesting results have been obtained between shrinking and stretching surface and also between the nanofluids (Cu, Al_2O_3 and TiO_2-water). Dimensionless velocity and temperature profiles have been obtained by varying magnetic field strength, heat source/sink, Eckert number and thermal radiation keeping volume concentration, porous parameter, suction/injection parameter and Grashof number constant.

a) In the presence of injection/suction, the retarding force produced by magnetic strength has more effect on TiO_2 and Al_2O_3-water nanofluid which is evident in velocity profiles.
b) TiO_2-water nanofluid has high temperature profile for heat source and Eckert number in the presence of injection when the flow over the shrinking surface.
c) Temperature profiles obtained in the presence of injection is higher than that of the suction.
d) Shrinking surface has high temperature profiles than the stretching surface for both injection/suction.
e) Cu-water nanofluid has high temperature distribution in the presence of suction.
f) TiO_2-water nanofluid has poor heat transfer rate over stretching surface in the presence of both suction and injection.

Analysing the results, Copper nanofluids has stable and reliable temperature profiles for all conditions and high thermal conductivity. There is no consistency in TiO_2 and Al_2O_3 nanofluids as their respective profiles show high or less temperature profiles, depending on governing parameters. TiO_2 nanoparticles are highly harmful when came in direct contact. Hence, Copper nanofluid is suitable for stagnation-point flow over a permeable surface.

NOMENCLATURE

Al_2O_3	Aluminium oxide nanoparticle
a,c	Constant (+ve)
B_0	Magnetic field strength
Cp_s	Specify heat of solid
Cp_f	Specific heat of fluid
Cp_{nf}	Specific heat of nanofluids
Cu	Copper nanoparticle
Ec	Eckert number
$f'(\eta)$	Dimensionless velocity

Gr Grashof number
g Gravitational force
K Porous parameter
K_1 Permeability of the porous medium (m^2)
K^* Mean spectral absorption coefficient (m^{-1})
M Magnetic field strength parameter ($Nm\ \Omega^{-1}A^{-2}\ s^{-1}$)
MHD Magnetohydrodynamics
N Thermal radiation parameter (s^3m^{-2})
ODE Ordinary differential equations
PDE Partial differential equations
Pr Prandtl number
Q_o Dimensional heat generation/absorption coefficient ($kgm^{-1}s^{-3}K^{-1}$)
Re Reynolds number
S Injection velocity parameter
TiO_2 Titanium dioxide nanoparticle
T_f Fluid Temperature
T_∞ Free stream temperature
T_w Wall temperature
u, v Velocity components in x,*y*-directions respectively
u_w Stretching or shrinking surface velocity
v_w Injection velocity
U Free stream velocity of the nanofluid
2-D Two-dimensional

Greek symbols

α_{nf} T hermal diffusivity of the nanofluid
α_f Fluid thermal diffusivity
β Thermal expansion coefficient
γ Buoyancy parameter
η Similarity variable
$\theta(\eta)$ Dimensionless temperature of the fluid
θ_w Wall temperature excess ratio parameter
$\theta'(\eta)$ Dimensionless heat transfer rate
κ Thermal conductivity
κ_f Thermal conductivity of the fluid
κ_{nf} Effective thermal conductivity of the nanofluid
κ_s Thermal conductivity of solid
λ Heat sink/source parameter
μ_f Dynamic viscosity of the fluid
μ_{nf} Effective dynamic viscosity of the nanofluid
ρ_f Density of fluid
ρ_{nf} Effective density of the nanofluid
ρ_s Density of solid
$(\rho C_p)_f$ Heat capacitance of fluid
$(\rho Cp)_{nf}$ Heat capacitance of nanofluid
$(\rho C_p)_s$ Heat capacitance of solid
σ Electrical conductivity
σ^* Stefan–Boltzmann constant
ϕ Nanoparticles volume fraction
Stream function

Superscripts

′ Differentiate with respect to x, y and η correspondingly

Subscripts

f Fluid
nf Nanofluid
s Solid

ACKNOWLEDGEMENT

The work was partly supported by Universiti Tun HusseinOnn Malaysia, Johor, Malaysia, under the Research Acculturation Grant Scheme (RAGS) Vot. R057

REFERENCES

Choi, S. 1995. Enhancing thermal conductivity of fluids with nanoparticle, development and applications of non-Newtonian flow, ASME FED, 231/MD *(66)*, pp. 99–105.

Duangthongsuk, W. and Wongwises,S. 2009. Heat transfer enhancement and pressure drop characteristics of TiO2–water nanofluid in a double-tube counter flow heat exchanger. International Journal of Heat and Mass Transfer, 52, pp. 2059–2067.

Fang, T.G., Zhang,J. and Yao, S.S. 2009. Viscous flow over an unsteady shrinking sheet with mass transfer. Chinese Physics Letters, 26(1), pp. 014703.

Hamad, M.A.A. and Pop, I. 2010. Scaling transformations for boundary layer flow near the stagnation-point on a heated permeable stretching surface in a porous medium saturated with a nanofluid and heat generation/absorption effects. Transport in Porous Medium, 87, pp. 25-39.

Heris, S.Z., Esfahany, M.N. and Etemad, S.G. 2006) Experimental investigation of oxide nanofluids laminar flow convective heat transfer. International Communications in Heat and Mass Transfer, 33(4), pp. 529-535.

Heris, S.Z., Esfahany, M.N. and Etemad, S.G. 2007. Experimental investigation of convective heat transfer of Al2O3/water nanofluid in circular tube.International Journal of Heat and Fluid Flow, 28(2), pp. 203.

Ibrahim, W., Shankar, B. and Nandeppanavar, M.M. 2013. MHD stagnation point flow and heat transfer due to nanofluid towards a stretching sheet. International Journal of Heat and Mass Transfer, 56, pp. 1-9.

Mahapatra, T.R. and Gupta, A.S. (2002). Heat transfer in stagnation-point flow towards a stretching sheet. Heat Mass Transfer. 38, pp. 517-521.

Mostafa, M., Hayat, T., Pop, I., Asghar, S. and Obaidat, S. 2011. Stagnation point flow of a nanofluid towards a stretching sheet. International Journal of Heat and Mass Transfer, 54, pp. 5588-5594.

Oztop, H. F. and Abu-Nada, E. 2008. Numerical study of natural convection in partially heated rectangular

enclosures filled with nanofluids. International Journal of Heat Fluid Flow, *29,* pp. 1326-1336.

Pak, B.C. andCho, Y.I. 1998. Hydrodynamic and heat transfer study of dispersed fluids with submicron metallic oxide particles.Experimental Heat Transfer, 11(2), pp. 151-170.

Pal, D., Mandal, G. and Vajravelu, K. 2014. Flow and heat transfer of nanofluids at a stagnation point flow over a stretching/shrinking surface in a porous medium with thermal radiation. Applied Mathematics and Computation, 238, pp.208-224.

Wang C.Y. 2008. Stagnation flow towards a shrinking sheet. International Journal of Non-Linear Mechanics, 43, pp. 377-382.